

Guided and Fused: Efficient Frozen CLIP-ViT with Feature Guidance and Multi-Stage Feature Fusion for Generalizable Deepfake Detection

Yingjian Chen¹, Lei Zhang¹, Yakun Niu^{1*}, Pei Chen¹, Lei Tan¹, Jing Zhou²

¹Henan Key Laboratory of Big Data Analysis and Processing, Henan University

²International Business School, Henan University

{yingjianchen, zhanglei, ykn, chenpei, tanlei}@henu.edu.cn, 10240053@vip.henu.edu.cn

Abstract

The rise of generative models has sparked concerns about image authenticity online, highlighting the urgent need for an effective and general detector. Recent methods leveraging the frozen pre-trained CLIP-ViT model have made great progress in deepfake detection. However, these models often rely on visual-general features directly extracted by the frozen network, which contain excessive information irrelevant to the task, resulting in limited detection performance. To address this limitation, in this paper, we propose an efficient Guided and Fused Frozen CLIP-ViT (GFF), which integrates two simple yet effective modules. The Deepfake-Specific Feature Guidance Module (DFGM) guides the frozen pre-trained model in extracting features specifically for deepfake detection, reducing irrelevant information while preserving its generalization capabilities. The Multi-Stage Fusion Module (FuseFormer) captures low-level and high-level information by fusing features extracted from each stage of the ViT. This dual-module approach significantly improves deepfake detection by fully leveraging CLIP-ViT's inherent advantages. Extensive experiments demonstrate the effectiveness and generalization ability of GFF, which achieves state-of-the-art performance with optimal results in only 5 training epochs. Even when trained on only 4 classes of ProGAN, GFF achieves nearly 99% accuracy on unseen GANs and maintains an impressive 97% accuracy on unseen diffusion models.

Introduction

Recently, the rapid rise of AI-generated content (AIGC) has attracted significant public interest. Especially in the field of image synthesis, society is facing unprecedented challenges due to the rapid development of the technology. The widespread adoption of advanced techniques like Generative Adversarial Networks (GANs) (Goodfellow et al. 2014) and diffusion models (Rombach et al. 2022) has made it effortless to produce highly realistic fake images. This rapid technological advancement has marked the end of the era where “seeing is believing.” These convincingly realistic images are becoming increasingly difficult to distinguish with human vision alone, posing significant risks to societal security. Consequently, effectively identifying such synthetic images has become an urgent concern.

*Corresponding author

Copyright © 2025, Association for the Advancement of Artificial Intelligence (www.aaai.org). All rights reserved.

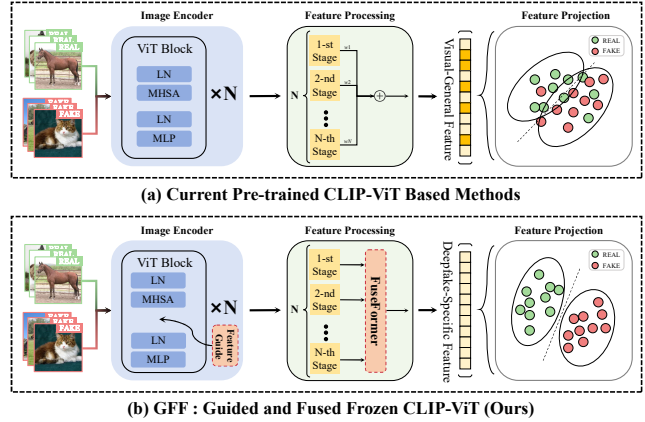


Figure 1: Comparison with existing methods. (a) CLIP-ViT-based methods that utilize visual-general features extracted from the frozen network, such as RINE (Koutlis and Papadopoulos 2024) and UniFD (Ojha, Li, and Lee 2023). (b) Our approach guides the frozen CLIP-ViT to extract deepfake-specific features and fully leverage them by incorporating two simple and efficient modules into the network.

In contrast to traditional methods that are dependent on manual feature extraction and handcrafted algorithms, existing deep learning-based detection methods have achieved remarkable success in detecting synthetic images. Ju et al. (Ju et al. 2023) and Tan et al. (Tan et al. 2024a) attain superior classification performance by carefully designing network architectures to capture important image features for deepfake detection. The methods (Tan et al. 2023; Liu et al. 2022a; Tan et al. 2024b) aim to discover more effective artifact representations, directly feeding them into existing networks such as ResNet50 (He et al. 2016) for synthetic image detection. However, the major issue with the current methods lies in the generalization of the model, some methods achieve excellent accuracy on the training set but suffer significant performance degradation on unseen datasets. As forgery techniques evolve, enhancing the generalization of models has become a critical challenge in deepfake detection. To address this problem, Ojha et al. (Ojha, Li, and Lee 2023) use a frozen pre-trained network to extract universal feature representations, keeping the weights unchanged dur-

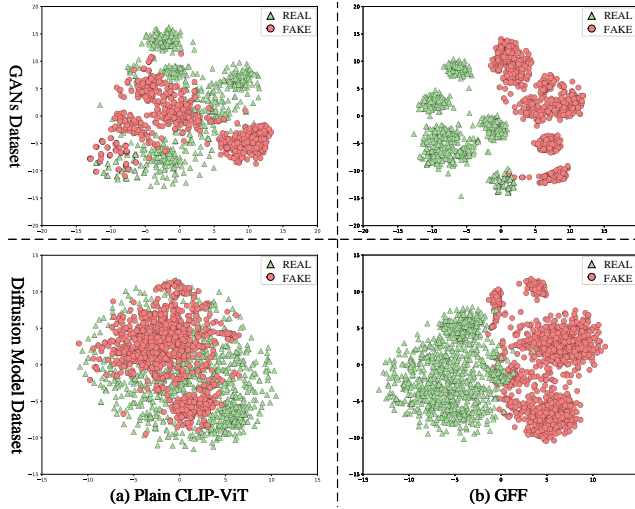


Figure 2: Feature space visualization for unseen GANs and diffusion model data using t-SNE. This highlights the differences between the features extracted by the plain CLIP-ViT (as utilized in methods like UniFD (Ojha, Li, and Lee 2023) and RINE (Koutlis and Papadopoulos 2024)) and our proposed method.

ing training. By leveraging CLIP-ViT (Radford et al. 2021) pre-trained on a large and diverse dataset, the model learns effective and generalizable features that help prevent overfitting and enhance generalization, thereby achieving decent detection accuracy.

However, since this method, along with recent approaches based on it, keeps the weights of CLIP-ViT unchanged during training (Figure 1 (a)), we speculate that the extracted features are visual-general rather than deepfake-specific. These features contain too much information irrelevant to deepfake detection, making it difficult for the classifier to focus on the subtle distinctions needed to differentiate forgery from real images. To investigate, we visualized the features extracted by the plain frozen pre-trained CLIP-ViT and GFF on unseen GANs and diffusion model data, as shown in Figure 2. The features extracted by the plain frozen CLIP-ViT are scattered, indicating they are general image features resulting from CLIP’s pre-training on a large-scale dataset. This observation supports our speculation.

Furthermore, recent studies, such as RINE (Koutlis and Papadopoulos 2024), utilize features extracted from intermediate Transformer modules to incorporate the low-level features essential for effective forgery detection. However, it still processes the general image features from the frozen CLIP-ViT, which are not specifically tailored for deepfake detection. In addition, FatFormer (Liu et al. 2024) simultaneously considers image features and text prompt embeddings. It introduces a forgery-aware adapter within the image encoder to capture forgery traces in both the spatial and frequency domains. However, the added complexity of the adapter may lead to noise or information loss during feature processing, potentially affecting the generalization advantage of the pre-trained CLIP-ViT.

Based on the above analysis, our motivation is to optimize feature extraction for deepfake detection by leveraging CLIP-ViT’s inherent strengths. We aim to guide the frozen pre-trained CLIP-ViT to autonomously extract deepfake-specific features by introducing a minimal number of trainable parameters. To achieve this, we propose Guided and Fused Frozen CLIP-ViT (GFF), illustrated in Figure 1 (b). Unlike previous methods that rely on the visual-general features (Figure 2 (a)) extracted by frozen pre-trained CLIP-ViT, we introduce a simple, trainable Deepfake-Specific Feature Guidance Module (DFGM) within the Vision Transformer (ViT) blocks to guide the model in learning deepfake-specific features (Figure 2 (b)) and reducing irrelevant information. Furthermore, we design a Transformer-based feature fusion network, FuseFormer, to integrate the multi-stage features extracted by the preceding network, ensuring that the extracted features are fully utilized. This approach leverages the generalization advantages of the frozen pre-trained CLIP-ViT while employing simple modules and reducing computational complexity.

The main contributions are summarized as follows:

- We introduce a novel CLIP-ViT-based architecture, GFF, designed for deepfake detection. Our approach guides the frozen pre-trained CLIP-ViT to learn deepfake-specific features and integrates multi-stage features extracted by the network, fully leveraging CLIP-ViT’s powerful pre-trained weights.
- We design a simple yet effective Deepfake-Specific Feature Guidance Module (DFGM) and integrate it into the basic CLIP-ViT blocks. During the training phase, only the DFGM is made trainable, guiding the frozen pre-trained network to autonomously learn features specifically for deepfake detection.
- We propose a multi-stage feature fusion module, called FuseFormer, to integrate the multi-stage features extracted from pre-trained CLIP-ViT. This module effectively combines low-level and high-level features, fully utilizing the features extracted by the pre-trained network.

Extensive experiments show that our method achieves state-of-the-art performance in several experimental scenarios, outperforming FatFormer, which considers both image and text, by effectively guiding frozen pre-trained CLIP-ViT to extract deepfake-specific features.

Related Work

Recently, deepfake detection methods have primarily focused on two aspects: preprocessing image data to highlight forgery artifacts and designing models to capture crucial features.

Data Preprocessing Based Methods

The focus of these methods is to enhance image representation or find new feature representations with improved robustness and generalization ability by applying image preprocessing, and then feeding them into popular classification networks, such as Resnet50 (He et al. 2016). Wang et al.

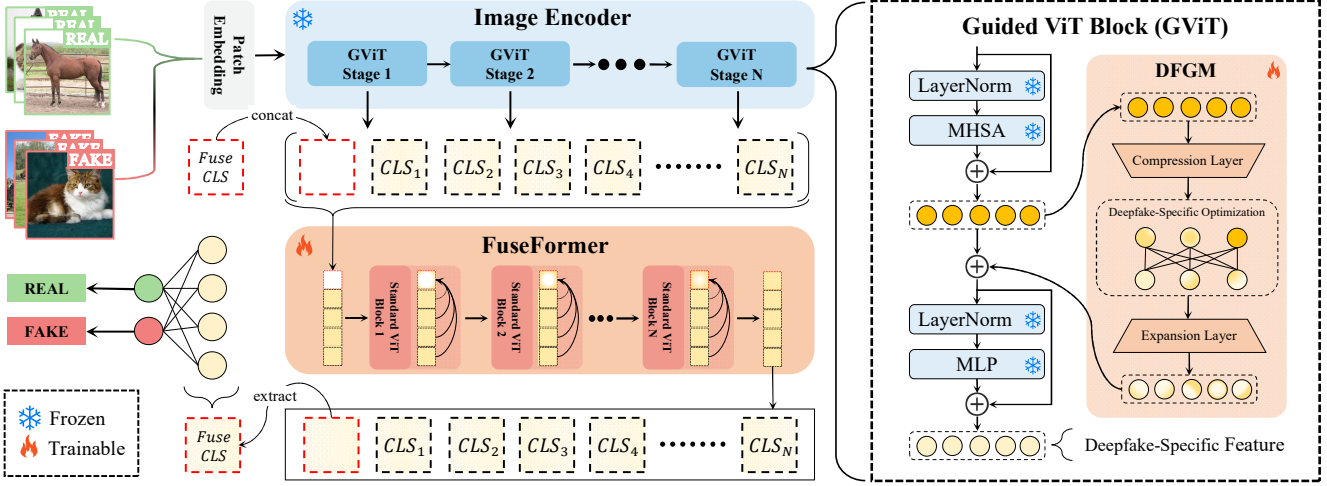


Figure 3: Our GFF architecture. The trainable DFGM is integrated into the plain vision transformer block, forming a new structure called GVIT (depicted by the blue rectangle in the Image Encoder), which guides the frozen ViT in learning deepfake-specific features; The CLS tokens (yellow square) extracted from each stage of the GVIT are concatenated with a Fuse CLS token (red square) and forwarded to FuseFormer (represented by the red rectangle), which consists of standard ViT blocks and is designed for multi-stage feature fusion; The resulting Fuse CLS token serves as the final feature for classification. The squares “Fuse CLS” and “ CLS_i ” represent the added Fuse CLS token and the image CLS token output by the i -th stage of the GVIT, respectively.

(Wang et al. 2020) employ diverse data augmentation techniques to enhance generalization to unseen testing data. Liu et al. (Liu et al. 2022a) identified a distinctive pattern in real images, referred to as Learned Noise Patterns, which exhibit stronger discrimination. Jeong et al. (Jeong et al. 2022b) propose a novel framework, FreGAN, integrating frequency-level perturbation maps to mitigate overfitting caused by unique artifacts in generated images, thereby enhancing detection accuracy across diverse test scenarios. BiHPF (Jeong et al. 2022a) amplifies the influence of frequency-level artifacts typically found in synthesized images from generative models using Bilateral High-Pass Filters. LGrad (Tan et al. 2023) transforms RGB images into their gradients through a transformation model, with these gradients serving as a general feature representation. NPR (Tan et al. 2024b) highlights the traces left by upsampling in forged images.

Model Based Methods

These kinds of methods mainly involve carefully designing an end-to-end network architecture to extract key features of images for deepfake detection. Gram-Net (Liu, Qi, and Torr 2020) designs Gram Blocks to extract global image texture representations for robust forgery face detection. Luo et al. (Luo et al. 2021) proposed a generalizable model that leverages both color texture and high-frequency noise from images to enhance generalization performance. GLFF (Ju et al. 2023) fuses multi-scale global features and local detail features extracted by a dual-branch network. Tan et al. (Tan et al. 2024a) propose FreNet that integrates frequency domain learning into CNN classifiers, forcing detectors to learn frequency domain features. NAFID (Deng et al. 2023) extracts the non-local features of images through a dedicated module. Furthermore, to address the problem of de-

creased model detection accuracy on other unseen forgery methods, Ojha et al. (Ojha, Li, and Lee 2023) leverage frozen pre-trained CLIP-ViT combined with a learnable linear layer that achieved astonishing generalization. Building on that, RINE (Koutlis and Papadopoulos 2024) leverages the image representations extracted by intermediate Transformer Blocks of CLIP-ViT. Khan et al. (Khan and Dang-Nguyen 2024) explore four transfer learning strategies and demonstrate that considering both CLIP’s image and text components together achieves improved performance. Liu et al. (Liu et al. 2024) introduce a forgery-aware adapter for forgery adaption and consider contrastive learning between image and text prompts used in CLIP.

Methodology

Overview

The overall framework of our method is illustrated in Figure 3. It consists of three major components: the CLIP-ViT as the backbone, a Deepfake-Specific Feature Guidance Module (DFGM), and a Transformer-Based Multi-Stage Fusion Module, which we refer to as FuseFormer.

CLIP-ViT

Benefiting from CLIP’s powerful pre-trained weights and efficient feature extraction capabilities, we adopt its frozen image encoder CLIP-ViT (Radford et al. 2021) as our pre-trained feature extractor, following the strategy outlined in UniFD (Ojha, Li, and Lee 2023). This approach integrates the Vision Transformer (ViT) (Dosovitskiy et al. 2020) as an image encoder, ensuring high-quality feature extraction while mitigating overfitting risks during feature guidance. Given an RGB image $x \in \mathbb{R}^{H \times W \times 3}$, the patch embedding layer splits and transforms it into a sequence of image

embeddings $E_{img} \in \mathbb{R}^{(N+1) \times D}$. Subsequently, the image embeddings are further processed through multiple Vision Transformer blocks, and the output CLS token is taken as the image encoding vector $f_i \in \mathbb{R}^{1 \times D}$. In this context, H and W denote the height and width of the image, 1 represents the CLS token, D represents projected D-dimensional image features, $N = \frac{HW}{P^2}$ denotes patch number, f_i represents i -th stage output of CLIP-ViT.

Deepfake-Specific Feature Guidance Module

To address the issue that directly using frozen pre-trained CLIP-ViT extracts visual-general features with excessive irrelevant information, which introduces noise and affects detection performance, we propose a lightweight and trainable Deepfake-Specific Feature Guidance Module (DFGM).

Given that the MHSA module processes the global features of the input while the MLP module further refines and nonlinearly transforms these features, we place the trainable DFGM between the MHSA and MLP modules. The DFGM optimizes the global features by learning deepfake-specific features and integrating them with the original features. Consequently, the features fed into the MLP are already optimized for deepfake detection, and further processing by the MLP allows the pre-trained model to extract deepfake-specific features more effectively. The process can be formulated as follows:

$$\begin{aligned} z &= MHSA(LN(x_{l-1})) + x_{l-1} \\ z' &= DFGM(z) + z \\ x_l &= MLP(LN(z')) + z' \end{aligned} \quad (1)$$

where $MHSA$ and MLP denote multi-head self-attention and multi-layer perceptron in classic ViT block, $DFGM$ represents the trainable deepfake-specific feature guidance module, and LN stands for layer normalization. x_l , z , z' represent the output features of the MLP , $MHSA$, and $DFGM$ modules in the l -th ViT block, respectively. This approach effectively filters out irrelevant information and guides the frozen CLIP-ViT to focus on features related to deepfake detection.

To reduce the number of trainable parameters and thereby preserve the inherent generalization advantages of the original frozen network, the DFGM module adopts a bottleneck structure. It comprises down and up projection layers, ReLU layers, and an additional linear layer specifically integrated to capture richer forgery artifacts for enhanced feature extraction, which can be represented as:

$$DFGM(z) = W_{up} \cdot \text{ReLU}(W_{mid} \cdot \text{ReLU}(W_{down} \cdot z)) \quad (2)$$

where $W_{down} \in \mathbb{R}^{d \times \hat{d}}$, $W_{up} \in \mathbb{R}^{\hat{d} \times d}$ denotes down and up projection, \hat{d} is the bottleneck middle dimension which satisfies $\hat{d} \ll d$, $W_{mid} \in \mathbb{R}^{\hat{d} \times \hat{d}}$ denote the additional middle linear layer. This down-up bottleneck architecture allows for the extraction of deepfake-specific features without compromising the features extracted by the pre-trained CLIP-ViT, thereby maximizing the utilization of its powerful generalization capabilities.

The DFGM module effectively guides the pre-trained model to extract deepfake-specific features that are highly relevant for deepfake detection task, while preserving the model's generalization benefits.

FuseFormer

After guiding the extraction of deepfake-specific features using the frozen CLIP-ViT, we intend to fully utilize the extracted features to further explore the potential of the pre-trained model. To achieve this, we integrate its multi-stage outputs to leverage both the low-level and high-level features.

Building on the finding that the classical Transformer leverages the CLS token to capture a comprehensive representation of the input sequence, this mechanism enables the Transformer to integrate diverse feature representations into a unified embedding. The CLS token, serving as a global representation, incorporates information from all input tokens during the self-attention process, effectively capturing the intricate relationships among various features. Furthermore, we observed that the output CLS tokens $CLS_i \in \mathbb{R}^D$ from each stage of the frozen ViT model inherently satisfy the input requirements of a Transformer, eliminating the need for additional embedding transformations. Consequently, we concatenated the CLS tokens from each stage and appended a new Fuse CLS token $CLS_{fuse} \in \mathbb{R}^D$, which serves as a comprehensive global representation of all stage outputs. This composite representation is expressed as:

$$c_0 = [CLS_{fuse}; CLS_1; CLS_2; \dots; CLS_N] \quad (3)$$

Based on this, we developed FuseFormer, a Transformer-based feature fusion module designed to integrate multi-stage features. The module employs the standard vision transformer block architecture (Dosovitskiy et al. 2020), the process can be easily demonstrated as follows:

$$\begin{aligned} c_l' &= MHSA(LN(c_{l-1})) + c_{l-1} \\ c_l &= MLP(LN(c_l')) + c_l' \end{aligned} \quad (4)$$

where $MHSA$ and MLP stand for multi-head self-attention and multi-layer perceptron in standard vision transformer block. c_l' , c_l represent the output features of the $MHSA$ and MLP modules for standard ViT block l , respectively.

The FuseFormer leverages the Transformer's self-attention mechanism to effectively fuse multi-stage features extracted from the frozen network, combining low-level and high-level information. Low-level features capture fine details and textures, while high-level features provide abstract information. By integrating these diverse features, FuseFormer further enhances deepfake detection performance by ensuring that extracted features are fully utilized.

Experiments

Datasets

To ensure a fair and consistent comparison, we follow existing methods by using only ProGAN-generated images for training and testing on unseen data. Therefore, we utilize

Methods	Year	Class	Test Models								
			ProGAN	StyleGAN	StyleGAN2	BigGAN	CycleGAN	StarGAN	GauGAN	Deepfake	Mean
Wang	2020	1	50.4/63.8	50.4/79.3	68.2/97.4	50.2/61.3	50.0/52.9	50.0/48.2	50.3/67.6	50.1/51.5	52.5/64.9
BiHPF	2022	1	82.5/81.4	68.0/62.8	68.8/63.6	67.0/62.5	75.5/74.2	90.1/90.1	73.6/92.1	51.6/49.9	72.1/72.1
FrePGAN	2022	1	95.5 99.4	80.6/90.6	77.4/93.0	63.5/60.5	59.4/59.9	<u>99.6/100.0</u>	53.0/49.1	70.4/81.5	74.9/79.3
LGrad	2023	1	<u>99.4/99.9</u>	96.0/99.6	93.8/99.4	79.5/88.9	84.7/94.4	99.5/100.0	70.9/81.8	66.7/77.9	86.3/92.7
UniFD	2023	1	99.1/100.0	77.2/95.9	69.8/95.8	94.5/99.0	97.1/99.9	98.0/100.0	95.7/100.0	82.4/91.7	89.2/97.8
FreqNet	2024	1	98.0/99.9	<u>92.0/98.7</u>	<u>89.5/97.9</u>	85.5/93.1	96.1/99.1	94.2/98.4	91.8/99.6	69.8/94.4	89.6/97.6
RINE	2024	1	99.8/100.0	88.7/99.1	86.9/99.7	99.1/99.9	<u>99.4/100.0</u>	98.8/100.0	99.7/100.0	82.7/97.4	94.4/99.5
Ours	-	1	99.8/100.0	84.4/99.5	84.3/99.7	<u>98.5/99.9</u>	99.7/100.0	100.0/100.0	<u>99.4/100.0</u>	94.6/98.6	95.1/99.7
Wang	2020	2	64.6/92.7	52.8/82.8	75.7/96.6	51.6/70.5	58.6/81.5	51.2/74.3	53.6/86.6	50.6/51.5	57.3/79.6
BiHPF	2022	2	87.4/87.4	71.6/74.1	77.0/81.1	82.6/80.6	86.0/86.6	93.8/80.8	75.3/88.2	53.7/54.0	78.4/79.1
FrePGAN	2022	2	99.0/99.9	80.8/92.0	72.2/94.0	66.0/61.8	69.1/70.3	98.5/100.0	53.1/51.0	62.2/80.6	75.1/81.2
LGrad	2023	2	<u>99.8/100.0</u>	<u>94.8/99.7</u>	<u>92.4/99.6</u>	82.5/92.4	95.9/94.7	99.7/99.9	73.7/83.2	60.6/67.8	86.2/92.2
UniFD	2023	2	99.7/100.0	78.8/97.4	75.4/96.7	91.2/99.0	91.9/99.8	96.3/99.9	91.9/100.0	80.0/89.4	88.1/97.8
FreqNet	2024	2	99.6/100.0	90.4/98.9	85.8/98.1	89.0/96.0	96.7/99.8	97.5/100.0	88.0/98.8	80.7/92.0	91.0/97.9
RINE	2024	2	<u>99.8/100.0</u>	84.9/99.5	76.7/99.6	<u>98.3/99.9</u>	<u>99.4/100.0</u>	<u>99.6/100.0</u>	99.9/100.0	66.7/96.4	90.6/99.4
FatFormer	2024	2	<u>99.8/100.0</u>	87.7/97.4	91.1/99.3	98.9/99.9	99.9/100.0	100.0/100.0	99.9/100.0	<u>89.4/97.3</u>	95.8/99.2
Ours	-	2	100.0/100.0	98.9/100.0	99.3/99.9	94.2/99.9	96.9/100.0	93.5/100.0	<u>95.7/100.0</u>	93.5/98.0	96.5/99.7
Wang	2020	4	91.4/99.4	63.8/91.4	76.4/97.5	52.9/73.3	72.7/88.6	63.8/90.8	63.9/92.2	51.7/62.3	67.1/86.9
BiHPF	2022	4	90.7/86.2	76.9/75.1	76.2/74.7	84.9/81.7	81.9/78.9	94.4/94.4	69.5/78.1	54.4/54.6	78.6/77.9
FrePGAN	2022	4	99.0/99.9	80.7/89.6	84.1/98.6	69.2/71.1	71.1/74.4	99.9/100.0	60.3/71.7	70.9/91.9	79.4/87.2
LGrad	2023	4	<u>99.9/100.0</u>	94.8/99.9	96.0/99.9	82.9/90.7	85.3/94.0	99.6/100.0	72.4/79.3	58.0/67.9	86.1/91.5
UniFD	2023	4	99.7/100.0	89.0/98.7	83.9/98.4	90.5/99.1	87.9/99.8	91.4/100.0	89.9/100.0	80.2/90.2	89.1/98.3
FreqNet	2024	4	99.6/100.0	90.2/99.7	88.0/99.5	90.5/96.0	95.8/99.6	85.7/99.8	93.4/98.6	88.9/94.4	91.5/98.5
NPR	2024	4	99.8/100.0	96.3/99.8	97.3/100.0	87.5/94.5	95.0/99.5	99.7/100.0	86.6/88.8	77.4/86.2	92.5/96.1
RINE	2024	4	100.0/100.0	88.9/99.4	94.5/100.0	99.6/99.9	<u>99.3/100.0</u>	99.5/100.0	99.8/100.0	80.6/97.9	95.3/99.7
FatFormer	2024	4	<u>99.9/100.0</u>	<u>97.2/99.8</u>	98.8/99.9	<u>99.5/100.0</u>	<u>99.3/100.0</u>	<u>99.8/100.0</u>	99.4/100.0	<u>93.2/98.0</u>	98.4/99.7
Ours	-	4	100.0/100.0	98.7/100.0	<u>98.7/99.8</u>	99.1/100.0	99.4/100.0	99.5/100.0	<u>99.5/100.0</u>	95.0/99.0	98.7/99.9

Table 1: Comparison of accuracy and average precision (ACC/AP) between our method and state-of-the-art techniques on the GANs dataset under three distinct training scenarios: 1-class, 2-class, and 4-class. The top-performing results are emphasized in bold, and the second-best results are underlined.

ForenSynths (Wang et al. 2020) training set to train our network following the current methods (Ojha, Li, and Lee 2023; Liu et al. 2024; Koutlis and Papadopoulos 2024). The ForenSynths training set contains 20 categories of real images from the LSUN dataset (Yu et al. 2015), and corresponding 20 categories of fake images generated by ProGAN (Karras et al. 2017). Consistent with the previous method, we use 1-class (horse), 2-class (chair, horse), and 4-class (car, cat, chair, horse) data to train our network. For evaluation, we employ the same testing GANs dataset and diffusion model dataset as FatFormer (Liu et al. 2024).

GANs Dataset. The GANs testing set adopts ForenSynths testing set, which includes images synthesized by eight forgery techniques: ProGAN (Karras et al. 2017), StyleGAN (Karras, Laine, and Aila 2019), StyleGAN2 (Karras et al. 2020), BigGAN (Brock, Donahue, and Simonyan 2018), CycleGAN (Zhu et al. 2017), StarGAN (Choi et al. 2018), GauGAN (Park et al. 2019) and Deepfake (Rossler et al. 2019).

Diffusion Model Dataset. The diffusion model dataset includes synthesized images generated by six generation models: PNDM (Liu et al. 2022b), Guided (Dhariwal and Nichol 2021), DALL-E (Radford et al. 2021), VQ-Diffusion (Gu et al. 2022), LDM (Rombach et al. 2022) and Glide (Nichol et al. 2021).

Evaluation metric

Following the standard procedures outlined in UniFD (Ojha, Li, and Lee 2023), RINE (Koutlis and Papadopoulos 2024), and FatFormer (Liu et al. 2024), we use accuracy (ACC) and average precision score (AP) as primary metrics to evaluate the effectiveness of our proposed method. To provide a comprehensive assessment of model performance across GAN and diffusion model datasets, we calculate the mean ACC and mean AP for each dataset.

Implementation Details

We employ a two-stage training methodology. In the first stage, we freeze the CLIP-ViT backbone network and train

Methods	Class	Test Models											Mean	
		PNDM	Guided	DALL-E	VQ-Diff	LDM			Glide					
						200 steps	200 w/CFG	100 steps	100-27	50-27	100-10			
Wang	4	50.8/90.3	54.9/66.6	51.8/61.3	50.0/71.0	52.0/64.5	51.6/63.1	51.9/63.7	53.0/71.3	54.2/76.0	53.3/72.9	52.4/70.1		
LGrad	4	69.8/98.5	86.6/100.0	88.5/97.3	96.3/100.0	94.2/99.1	95.9/99.2	94.8/99.2	87.4/93.2	90.7/95.1	89.4/94.9	89.4/97.7		
UniFD	4	75.3/92.5	75.7/85.1	89.5/96.8	83.5/97.7	90.2/97.1	77.3/88.6	90.5/97.0	90.7/97.2	91.1/97.4	90.1/97.0	95.4/94.6		
FatFormer	4	99.3/100.0	76.1/92.0	98.8/99.8	100.0/100.0	98.6/99.8	94.9/99.1	98.7/99.9	94.4/99.1	94.7/99.4	94.2/99.2	95.0/98.8		
Ours	1	64.9/97.9	79.9/96.5	94.9/99.9	70.2/99.9	96.9/99.8	86.6/99.3	97.0/99.8	84.2/99.2	88.5/99.5	87.2/99.6	85.0/99.1		
Ours	2	99.5/100.0	94.2/98.7	99.1/100.0	99.1/100.0	99.3/100.0	98.7/99.9	99.1/100.0	98.3/99.6	98.8/99.9	98.2/99.9	98.4/99.8		
Ours	4	93.8/99.5	88.4/98.5	99.7/100.0	99.6/100.0	99.6/100.0	98.6/100.0	99.7/100.0	98.4/99.9	98.8/99.9	98.5/99.9	97.5/99.8		

Table 2: Comparison of accuracy and average precision (ACC/AP) between our method, trained on three different scenarios (1-class, 2-class, and 4-class), and state-of-the-art techniques trained exclusively on the 4-class scenario using the diffusion model dataset.

only the DFGM. In the subsequent stage, we keep all preceding networks frozen and integrate FuseFormer into the backend, training it independently. In both stages, our experimental setup follows the methods outlined in previous works (Ojha, Li, and Lee 2023; Liu et al. 2024). Input images are resized to 256×256 and then cropped to a final resolution of 224×224 . During training, random cropping and horizontal flipping are applied, without additional augmentations. For testing, only center cropping is employed. We utilize the Adam optimizer (Kingma and Ba 2014) with beta parameters set to (0.9, 0.999), and apply standard binary cross-entropy as the loss function. In the first stage, the initial learning rate is set to 5×10^{-5} , with a training duration of 3 epochs and a total batch size of 32. During the second stage, the initial learning rate is reduced to 5×10^{-6} , with training limited to 1 epoch and a total batch size of 128. Experiments were conducted utilizing the PyTorch framework (Paszke et al. 2019) on a Nvidia GeForce RTX 3090 GPU.

Model Evaluation

To highlight the outstanding generalization capability of our model, we perform evaluations on both the GANs dataset and the diffusion model dataset. We primarily compare our model against previous methods that use the frozen pre-trained CLIP-ViT, such as UniFD (Ojha, Li, and Lee 2023), RINE (Koutlis and Papadopoulos 2024), and FatFormer (Liu et al. 2024). Additionally, to evaluate our model’s effectiveness, we compare it with other established methods, including BiHPF(Jeong et al. 2022a), FrePGAN (Jeong et al. 2022b), LGrad (Tan et al. 2023), FreqNet (Tan et al. 2024a), and NPR (Tan et al. 2024b).

Table 1 presents a comparison between our method and previous approaches on the GANs dataset under three training scenarios (1-class, 2-class, and 4-class). The results demonstrate that our proposed method outperforms existing methods in terms of mean accuracy (mACC) and mean average precision (mAP) across all scenarios. In the 4-class setting, our model achieves a mACC of 98.7%, showcasing superior performance compared to state-of-the-art pre-trained based methods such as RINE (Koutlis and Papadopoulos 2024) and FatFormer(Liu et al. 2024). Notably, our model

surpasses RINE, which also only considers the image encoder, by 3.4% in mACC. It even exceeds FatFormer, which integrates both text and image features, while utilizing fewer parameters and simpler modules. Furthermore, it is worth mentioning that even when our method is trained with only a single class of the ProGAN data, its mean ACC/AP remains comparable to the RINE method, which is trained with four types of data. This demonstrates the efficiency and effectiveness of our approach.

Furthermore, given that the generation mechanism of diffusion models is fundamentally different from that of GANs (Generative Adversarial Networks), we conducted a series of comparisons to further evaluate the effectiveness and generalization ability of our model. Specifically, we compared our model with existing detection methods on the diffusion model dataset, as presented in Table 2. All existing methods listed in the table were trained using four ProGAN classes, and our method was trained on 1, 2, and 4 classes to ensure a more comprehensive evaluation. After training on the ProGAN dataset, all methods were evaluated on diffusion models to assess their generalization capabilities. Our model demonstrates exceptional performance in this demanding setting, achieving a mean accuracy (ACC) of 97.5% and a mean precision (AP) of 99.8%. Compared to pre-trained-based methods such as UniFD (Ojha, Li, and Lee 2023) and FatFormer (Liu et al. 2024), our model performs better in detecting diffusion model forgeries. Specifically, it outperforms the state-of-the-art method FatFormer by 2.5% in mean ACC and 1.0% in mean AP. These results demonstrate the generalization ability and effectiveness of our approach, highlighting its significant advantages over existing methods. Additionally, it is noteworthy that our method achieved a mean accuracy of 98.4% on the diffusion model dataset when trained using only two types of ProGAN data. We speculate that less training data may mitigate the risk of overfitting complex data distributions and enhance the generalization ability to unseen diffusion model data.

Ablation Study

We performed ablation analyses by removing DFGM, FuseFormer, and both modules from our model. These experi-

GANs dataset			
	1-class	2-class	4-class
w/o Both	86.5 / 97.0	87.5 / 97.2	89.4 / 98.0
w/o DFGM	92.0 / 99.6	92.7 / 99.7	95.4 / 99.6
w/o FuseFormer	94.8 / 99.4	95.3 / 99.8	98.6 / 99.8
full	95.1 / 99.7	96.5 / 99.7	98.7 / 99.9

Diffusion model dataset			
	1-class	2-class	4-class
w/o Both	79.8 / 93.5	77.8 / 95.0	80.7 / 96.1
w/o DFGM	88.2 / 99.2	94.8 / 99.3	95.0 / 99.1
w/o FuseFormer	84.6 / 98.7	97.4 / 99.6	96.9 / 99.6
full	85.0 / 99.1	98.4 / 99.8	97.5 / 99.8

Table 3: Mean accuracy and mean average precision (mACC/mAP) in the Ablation Study of GFF on the GANs and diffusion model datasets across 1-class, 2-class, and 4-class training settings. Results without each module are denoted as 'w/o'. The top-performing results are highlighted in bold.

ments were conducted on the GANs dataset and the diffusion model dataset, across three training scenarios: 1-class, 2-class, and 4-class settings. The results of these experiments are detailed in Table 3. In nearly all scenarios, we observed that the mACC and mAP on both the GANs dataset and the diffusion model dataset decreased when each module was removed, highlighting the effectiveness of the proposed components. However, in the 1-class training scenario on the diffusion model dataset, performance improved after removing the DFGM but remained significantly higher than with the plain CLIP-ViT. This indicates a potential risk of overfitting to the single class in this specific case.

Class Activation Map Visualization

To further illustrate the differences between the visual-general features extracted by the plain frozen CLIP-ViT and the deepfake-specific features extracted by GFF, we performed class activation map (CAM) analysis of these two features on real images and those generated by StyleGAN, BigGAN, and Deepfake, as shown in Figure 4. This analysis reaffirms that the features extracted by the frozen pre-trained CLIP-ViT model are largely generic and suitable for various downstream tasks but lack specialization for deepfake detection. Consequently, the visual-general features from CLIP-ViT often fall short of accurately identifying forgery artifacts, as evidenced by the CAM analysis, which reveals a scattered focus and an inability to pinpoint specific forged regions. In contrast, the deepfake-specific features extracted by GFF focus on specific forged areas in deepfake images, such as hair and facial textures, demonstrating a more concentrated and targeted response. For instance, when detecting deepfakes, GFF significantly highlights the regions with face swap artifacts. The experimental results indicate that GFF effectively overcomes the limitations of the general features extracted by the frozen CLIP-ViT model, providing a more specialized feature representation that improves deepfake detection.

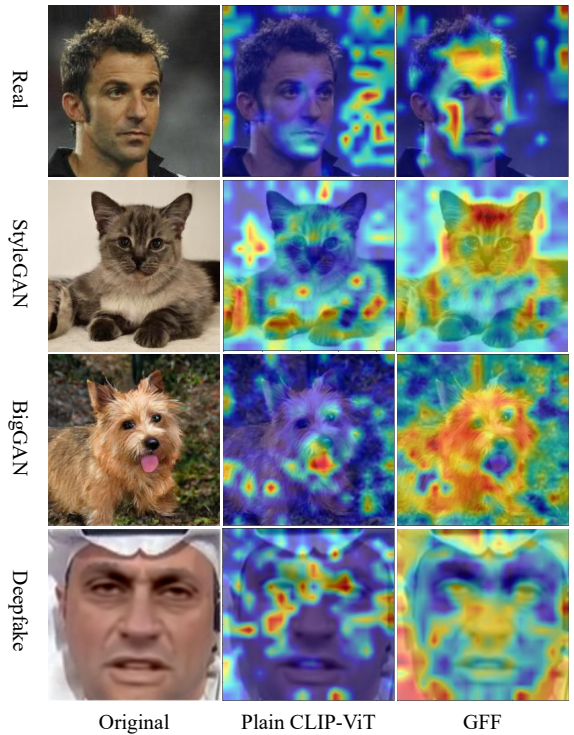


Figure 4: Class Activation Map (CAM) (Zhou et al. 2016) visualization of features extracted by the plain frozen CLIP-ViT and GFF.

Conclusion

In this study, we present a novel Guided and Fused Frozen CLIP-ViT called GFF, designed for generalizable image detection tasks. We introduced two simple yet highly effective modules into the plain CLIP-ViT. These modules guide the frozen CLIP-ViT to learn deepfake-specific features while fully utilizing its extracted features with a small number of trainable parameters. Extensive experiments on GANs and diffusion model datasets demonstrate that GFF achieves state-of-the-art performance on both, showcasing the strong generalization capability of our method. Furthermore, due to the simplicity and flexibility of the two modules in our approach, we hope it can inspire further advancements and improvements in the field of deepfake detection using frozen pre-trained models.

Limitations and Future Works

Admittedly, one unavoidable limitation of our method is its sensitivity to hyperparameters. Given the small and inadequately diverse dataset, the model tends to rely on specific features, amplifying this sensitivity. This challenge arises from the ongoing development of image synthesis technology, where models need to learn the distribution of synthetic images with limited data. Addressing this limitation will be a focus of future work to further enhance the model's performance.

Appendix

In this appendix, we provide supplementary materials that include the following: additional ablation studies to investigate the impact of various hyperparameters within our approach; robustness experiments to evaluate the effectiveness of our method in resisting different types of perturbations; additional CAM feature visualizations to illustrate further the effectiveness of the deepfake-specific features extracted by GFF; a presentation of the trainable parameters in our model.

Additional Ablation Studies

We conducted additional ablation studies to further investigate the hyperparameters used in our GFF, as shown in Table A1.

#bottleneck_dim	#FuseFormer_layers	mACC	mAP
64	1	95.0	99.6
	2	93.3	99.8
	4	94.9	99.7
	8	94.4	99.8
	16	93.5	99.8
128	1	96.6	99.8
	2	95.0	99.8
	4	97.2	99.8
	8	95.0	99.8
	16	95.6	99.7
256	1	96.4	99.9
	2	98.7	99.9
	4	98.3	99.8
	8	97.8	99.9
	16	98.1	99.9
512	1	92.3	99.6
	2	91.1	99.5
	4	85.6	99.4
	8	88.0	99.5
	16	86.3	99.5

Table A1: Additional ablation experiment results. The average accuracy (mACC) and average precision (mAP) of the GFF on the GANs dataset with different DFGM bottleneck dimensions and FuseFormer layers.

Bottleneck dimension of DFGM. We conducted an ablation study to explore the impact of different bottleneck dimensions in the Deepfake-specific Feature Guided Module (DFGM) on model performance. Our findings indicate that smaller bottleneck dimensions fail to effectively guide

Perturbation	Method	Class	mACC	mAP
Gaussian blurring	UniFD	4	78.1	93.0
	FatFormer	4	90.7	98.1
	Ours	4	93.1	99.5
Random cropping	UniFD	4	88.9	98.1
	FatFormer	4	98.2	99.7
	Ours	4	97.4	99.7
JPEG compression	UniFD	4	88.4	97.7
	FatFormer	4	95.9	99.2
	Ours	4	95.8	99.6
Gaussian noising	UniFD	4	82.6	93.9
	FatFormer	4	88.0	96.5
	Ours	4	88.7	99.1
Mean	UniFD	4	84.5	95.7
	FatFormer	4	93.2	98.4
	Ours	4	93.8	99.5

Table A2: Comparison of mean accuracy and mean average precision (mACC/mAP) between our method and state-of-the-art techniques, trained on four classes of the GANs dataset, following the application of various image perturbations.

the frozen pre-trained CLIP-ViT in focusing on deepfake-specific features. On the other hand, larger bottleneck dimensions can adversely affect the generalization capabilities of the pre-trained CLIP-ViT, disrupting the balance between leveraging its generalization benefits and guiding it to learn deepfake-specific features. Our experiments revealed that a bottleneck dimension of 256 presents the best performance. In this setting, the DFGM effectively leverages the generalization benefits of the pre-trained CLIP-ViT while guiding it to learn deepfake-specific features.

Number of FuseFormer layers. This ablation study aims to investigate the impact of different numbers of FuseFormer layers on model performance. Our analysis shows that fewer layers limit the model’s ability to effectively learn and integrate multi-stage features from CLIP-ViT. On the other hand, increasing the number of FuseFormer layers raises the risk of overfitting. Our experiments demonstrated that a FuseFormer layer count of 2 provides the optimal performance. This configuration achieves the best balance, allowing the model to effectively learn and fuse features from CLIP-ViT without overfitting.

Model Robustness Ability Evaluation

To evaluate the robustness of the model in real-world scenarios, we implemented a series of perturbations, following the methodology outlined by Frank et al.(Frank et al. 2020) and FatFormer(Liu et al. 2024). Specifically, we applied random cropping, Gaussian blur, JPEG compression, and Gaussian

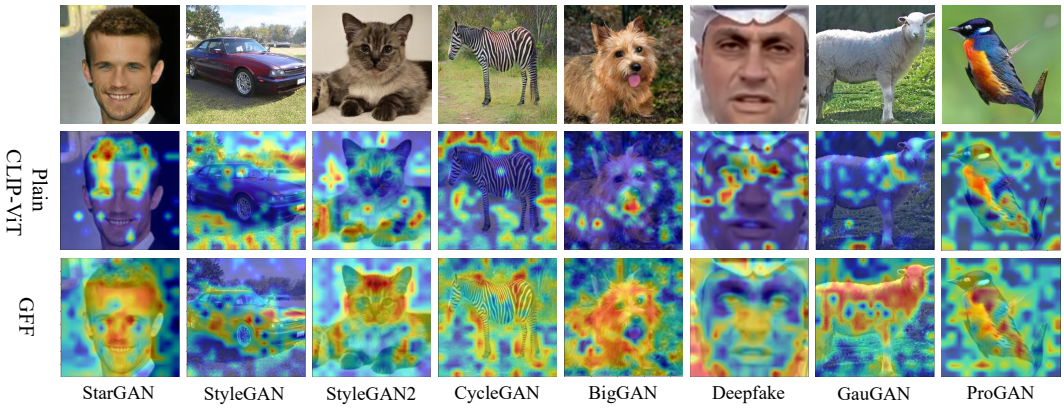


Figure A5: Class Activation Map (CAM) (Zhou et al. 2016) visualization of features extracted by the plain frozen CLIP-ViT and GFF on GANs dataset.

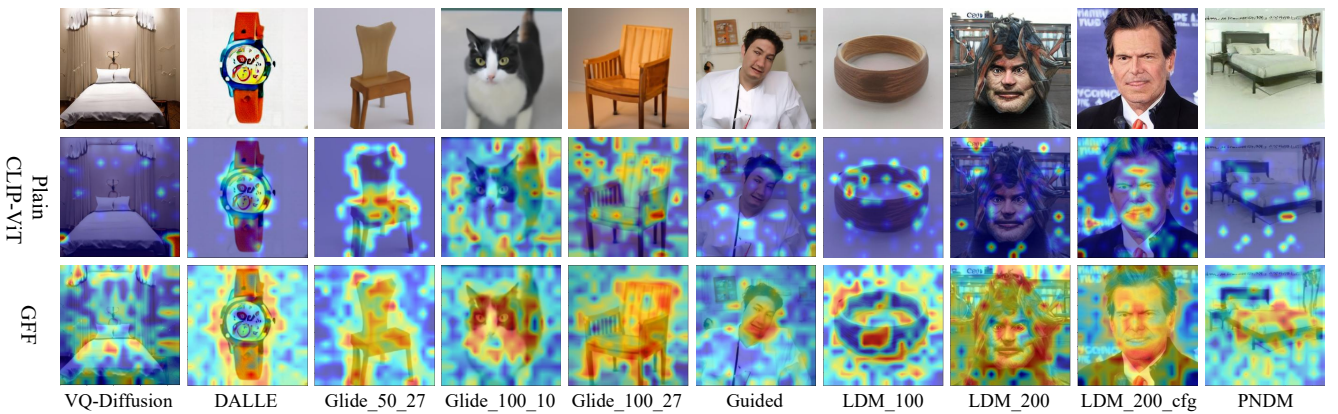


Figure A6: Class Activation Map (CAM) visualization of features extracted by the plain frozen CLIP-ViT and GFF on diffusion model dataset.

noise to the original image with a 50% probability. We conducted a comparative analysis on the GANs dataset to evaluate the robustness performance of our GFF method. This analysis included UniFD(Ojha, Li, and Lee 2023) and FatFormer(Liu et al. 2024), both of which leverage a frozen pre-trained CLIP-ViT. The results of this comparison are detailed in Table A2.

The results indicate that our proposed method surpasses current state-of-the-art techniques in most scenarios. However, the average accuracy of our method under random cropping and JPEG compression perturbations is slightly lower than that of FatFormer. Despite this minor discrepancy, our method demonstrates strong robustness overall.

Additional Class Activation Map Visualization

To more comprehensively validate the effectiveness of the deepfake-specific features extracted by GFF, we conducted extensive CAM visualizations on both the GANs dataset and the Diffusion model dataset, as illustrated in Figures A5 and A6. Compared to the visual-general features extracted using only the plain frozen pre-trained CLIP-ViT, the deepfake-specific features extracted by GFF exhibit more responses

and focus more on the specific forged regions within deepfake images.

Module Name	#Per Parameters	#Total Parameters
GFF-DFGM	0.59M	14.16M
FatFormer-FAA	16.93M	50.79M

Table A3: Trainable parameters (M) between our DFGM and FAA in FatFormer. #Per Parameters refers to the trainable parameters per module, while #Total Parameters denotes the total trainable parameters across all modules.

Trainable Parameters

To further validate the efficiency of our proposed DFGM module, we compared its parameters with those of the FAA module proposed in FatFormer(Liu et al. 2024), both within the image encoder, as shown in Table A3. The results indicate that our DFGM module introduces only 0.59M additional parameters to the plain CLIP-ViT block while achieving superior performance compared to FatFormer, demonstrating its high efficiency and effectiveness.

References

Brock, A.; Donahue, J.; and Simonyan, K. 2018. Large scale GAN training for high fidelity natural image synthesis. *arXiv preprint arXiv:1809.11096*.

Choi, Y.; Choi, M.; Kim, M.; Ha, J.-W.; Kim, S.; and Choo, J. 2018. Stargan: Unified generative adversarial networks for multi-domain image-to-image translation. In *Proceedings of the IEEE conference on computer vision and pattern recognition*, 8789–8797.

Deng, X.; Zhao, B.; Guan, Z.; and Xu, M. 2023. New finding and unified framework for fake image detection. *IEEE Signal Processing Letters*, 30: 90–94.

Dhariwal, P.; and Nichol, A. 2021. Diffusion models beat gans on image synthesis. *Advances in neural information processing systems*, 34: 8780–8794.

Dosovitskiy, A.; Beyer, L.; Kolesnikov, A.; Weissenborn, D.; Zhai, X.; Unterthiner, T.; Dehghani, M.; Minderer, M.; Heigold, G.; Gelly, S.; et al. 2020. An image is worth 16x16 words: Transformers for image recognition at scale. *arXiv preprint arXiv:2010.11929*.

Frank, J.; Eisenhofer, T.; Schönherr, L.; Fischer, A.; Kolossa, D.; and Holz, T. 2020. Leveraging frequency analysis for deep fake image recognition. In *International conference on machine learning*, 3247–3258. PMLR.

Goodfellow, I.; Pouget-Abadie, J.; Mirza, M.; Xu, B.; Warde-Farley, D.; Ozair, S.; Courville, A.; and Bengio, Y. 2014. Generative adversarial nets. *Advances in neural information processing systems*, 27.

Gu, S.; Chen, D.; Bao, J.; Wen, F.; Zhang, B.; Chen, D.; Yuan, L.; and Guo, B. 2022. Vector quantized diffusion model for text-to-image synthesis. In *Proceedings of the IEEE/CVF conference on computer vision and pattern recognition*, 10696–10706.

He, K.; Zhang, X.; Ren, S.; and Sun, J. 2016. Deep residual learning for image recognition. In *Proceedings of the IEEE conference on computer vision and pattern recognition*, 770–778.

Jeong, Y.; Kim, D.; Min, S.; Joe, S.; Gwon, Y.; and Choi, J. 2022a. Bihpf: Bilateral high-pass filters for robust deepfake detection. In *Proceedings of the IEEE/CVF Winter Conference on Applications of Computer Vision*, 48–57.

Jeong, Y.; Kim, D.; Ro, Y.; and Choi, J. 2022b. Freqgan: robust deepfake detection using frequency-level perturbations. In *Proceedings of the AAAI conference on artificial intelligence*, volume 36, 1060–1068.

Ju, Y.; Jia, S.; Cai, J.; Guan, H.; and Lyu, S. 2023. Glff: Global and local feature fusion for ai-synthesized image detection. *IEEE Transactions on Multimedia*.

Karras, T.; Aila, T.; Laine, S.; and Lehtinen, J. 2017. Progressive growing of gans for improved quality, stability, and variation. *arXiv preprint arXiv:1710.10196*.

Karras, T.; Laine, S.; and Aila, T. 2019. A style-based generator architecture for generative adversarial networks. In *Proceedings of the IEEE/CVF conference on computer vision and pattern recognition*, 4401–4410.

Karras, T.; Laine, S.; Aittala, M.; Hellsten, J.; Lehtinen, J.; and Aila, T. 2020. Analyzing and improving the image quality of stylegan. In *Proceedings of the IEEE/CVF conference on computer vision and pattern recognition*, 8110–8119.

Khan, S. A.; and Dang-Nguyen, D.-T. 2024. CLIPping the Deception: Adapting Vision-Language Models for Universal Deepfake Detection. *arXiv preprint arXiv:2402.12927*.

Kingma, D. P.; and Ba, J. 2014. Adam: A method for stochastic optimization. *arXiv preprint arXiv:1412.6980*.

Koutlis, C.; and Papadopoulos, S. 2024. Leveraging Representations from Intermediate Encoder-blocks for Synthetic Image Detection. *arXiv preprint arXiv:2402.19091*.

Liu, B.; Yang, F.; Bi, X.; Xiao, B.; Li, W.; and Gao, X. 2022a. Detecting generated images by real images. In *European Conference on Computer Vision*, 95–110. Springer.

Liu, H.; Tan, Z.; Tan, C.; Wei, Y.; Wang, J.; and Zhao, Y. 2024. Forgery-aware adaptive transformer for generalizable synthetic image detection. In *Proceedings of the IEEE/CVF Conference on Computer Vision and Pattern Recognition*, 10770–10780.

Liu, L.; Ren, Y.; Lin, Z.; and Zhao, Z. 2022b. Pseudo numerical methods for diffusion models on manifolds. *arXiv preprint arXiv:2202.09778*.

Liu, Z.; Qi, X.; and Torr, P. H. 2020. Global texture enhancement for fake face detection in the wild. In *Proceedings of the IEEE/CVF conference on computer vision and pattern recognition*, 8060–8069.

Luo, Y.; Zhang, Y.; Yan, J.; and Liu, W. 2021. Generalizing face forgery detection with high-frequency features. In *Proceedings of the IEEE/CVF conference on computer vision and pattern recognition*, 16317–16326.

Nichol, A.; Dhariwal, P.; Ramesh, A.; Shyam, P.; Mishkin, P.; McGrew, B.; Sutskever, I.; and Chen, M. 2021. Glide: Towards photorealistic image generation and editing with text-guided diffusion models. *arXiv preprint arXiv:2112.10741*.

Ojha, U.; Li, Y.; and Lee, Y. J. 2023. Towards universal fake image detectors that generalize across generative models. In *Proceedings of the IEEE/CVF Conference on Computer Vision and Pattern Recognition*, 24480–24489.

Park, T.; Liu, M.-Y.; Wang, T.-C.; and Zhu, J.-Y. 2019. Semantic image synthesis with spatially-adaptive normalization. In *Proceedings of the IEEE/CVF conference on computer vision and pattern recognition*, 2337–2346.

Paszke, A.; Gross, S.; Massa, F.; Lerer, A.; Bradbury, J.; Chanan, G.; Killeen, T.; Lin, Z.; Gimelshein, N.; Antiga, L.; et al. 2019. Pytorch: An imperative style, high-performance deep learning library. *Advances in neural information processing systems*, 32.

Radford, A.; Kim, J. W.; Hallacy, C.; Ramesh, A.; Goh, G.; Agarwal, S.; Sastry, G.; Askell, A.; Mishkin, P.; Clark, J.; et al. 2021. Learning transferable visual models from natural language supervision. In *International conference on machine learning*, 8748–8763. PMLR.

Rombach, R.; Blattmann, A.; Lorenz, D.; Esser, P.; and Ommer, B. 2022. High-resolution image synthesis with latent

diffusion models. In *Proceedings of the IEEE/CVF conference on computer vision and pattern recognition*, 10684–10695.

Rossler, A.; Cozzolino, D.; Verdoliva, L.; Riess, C.; Thies, J.; and Nießner, M. 2019. Faceforensics++: Learning to detect manipulated facial images. In *Proceedings of the IEEE/CVF international conference on computer vision*, 1–11.

Tan, C.; Zhao, Y.; Wei, S.; Gu, G.; Liu, P.; and Wei, Y. 2024a. Frequency-Aware Deepfake Detection: Improving Generalizability through Frequency Space Domain Learning. In *Proceedings of the AAAI Conference on Artificial Intelligence*, volume 38, 5052–5060.

Tan, C.; Zhao, Y.; Wei, S.; Gu, G.; Liu, P.; and Wei, Y. 2024b. Rethinking the up-sampling operations in cnn-based generative network for generalizable deepfake detection. In *Proceedings of the IEEE/CVF Conference on Computer Vision and Pattern Recognition*, 28130–28139.

Tan, C.; Zhao, Y.; Wei, S.; Gu, G.; and Wei, Y. 2023. Learning on gradients: Generalized artifacts representation for gan-generated images detection. In *Proceedings of the IEEE/CVF Conference on Computer Vision and Pattern Recognition*, 12105–12114.

Wang, S.-Y.; Wang, O.; Zhang, R.; Owens, A.; and Efros, A. A. 2020. CNN-generated images are surprisingly easy to spot... for now. In *Proceedings of the IEEE/CVF conference on computer vision and pattern recognition*, 8695–8704.

Yu, F.; Seff, A.; Zhang, Y.; Song, S.; Funkhouser, T.; and Xiao, J. 2015. Lsun: Construction of a large-scale image dataset using deep learning with humans in the loop. *arXiv preprint arXiv:1506.03365*.

Zhou, B.; Khosla, A.; Lapedriza, A.; Oliva, A.; and Torralba, A. 2016. Learning deep features for discriminative localization. In *Proceedings of the IEEE conference on computer vision and pattern recognition*, 2921–2929.

Zhu, J.-Y.; Park, T.; Isola, P.; and Efros, A. A. 2017. Unpaired image-to-image translation using cycle-consistent adversarial networks. In *Proceedings of the IEEE international conference on computer vision*, 2223–2232.